High sensitivity spectroscopy of the O2 band at 1.27 μm: (II) Air-broadened line profile parameters

Duc Dung Tran, Ha Tran, Semyon Vasilchenko, Samir Kassi, Alain Campargue, Didier Mondelain

Manuscript Details

Manuscript number	JQSRT_2019_433
Title	High sensitivity spectroscopy of the O2 band at 1.27 μm: (II) Air-broadened line profile parameters
Article type	Full Length Article

Abstract

A cavity ring down spectrometer referenced to a frequency comb is used to study the profile of air-broadened O2 lines of the 1.27 μm band. To this aim, spectra of O2 in dry air and of O2 in N2 with 2% of O2 were measured, respectively in the 7720-7920 cm−1 and 7868-7887 cm-1 spectral ranges at room temperature and various pressures ranging from 50 to 700 Torr. Detailed line profile analysis is reported for 85 transitions using the speed dependent Nelkin-Ghatak model and a multi-spectrum treatment of the two series of spectra. Line mixing was found necessary to be taken into account in the analysis of lines in the region of the Q branch. The derived line parameters including the broadening and shifting coefficients, the speed dependent components of the collisional line broadening and shifting, as well as the Dicke narrowing parameter are discussed and compared to literature data. In particular, the speed dependence components of the collisional broadening are found to agree satisfactorily with predictions obtained by molecular dynamic simulations. This obtained set of line-shape parameters should allow for improved modeling of atmospheric spectra in the 1.27 um spectral region.

Keywords	Oxygen band at 1.27 □m; Cavity ring-down spectroscopy; line intensity; line-shape; line mixing; speed-dependent Nelkin-Ghatak profile;

Corresponding Author	Tran Ha
Corresponding Author's Institution	CNRS, University Paris 6
Order of Authors	Duc Dung Tran, Tran Ha, Semyon Vasilchenko, Kassi Samir, Alain Campargue, Didier Mondelain

Suggested reviewers	Iouli Gordon, Daniel Lisak, Joseph Hodges, David Long

Submission Files Included in this PDF

File Name [File Type]

Cover_Letter.doc [Cover Letter]

Highlights.doc [Highlights]

Graphical abstract.tif [Graphical Abstract]

Manuscript_2507_reference_numerote.docx [Manuscript File]

To view all the submission files, including those not included in the PDF, click on the manuscript title on your EVISE Homepage, then click 'Download zip file'.

Laboratoire de Météorologie Dynamique

UMR 8539 – Université Pierre et Marie Curie – Sorbonne Université
Tour 45-55, 3ème étage, Case Postale 99
4, place Jussieu
F 75252 Paris Cedex 05, France
Tel : +33 (0)1 44 27 84 06 Fax : +33 (0)1 44 27 62 72
Web: http://www.lmd.jussieu.fr/

Journal of Quantitative Spectroscopy and Radiative Transfer

Paris July 25, 2019

Dear Editor,

Please find here our paper entitled "*High sensitivity spectroscopy of the O_2 band at 1.27 μm: (II) Air-broadened line profile parameters*" by D. D. Tran, me, S. Vasilchenko, S. Kassi, A. Campargue and D. Mondelain that we would like to submit to the Journal of Quantitative Spectroscopy and Radiative Transfer.

Sincerely yours,

Spectra of air-broadened O_2 in the 1.27 μm band were measured by CRDS referenced to a frequency comb

Line intensity and line-shape parameters were retrieved for 85 lines with the speed dependent Nelkin-Ghatak profile

Line-mixing effect was evidenced and measured for lines in the Q branch region

The results reveal several differences with data from HITRAN and existing studies

The retrieved high-order line-shape parameters are in good agreement with predictions from molecular dynamics simulations

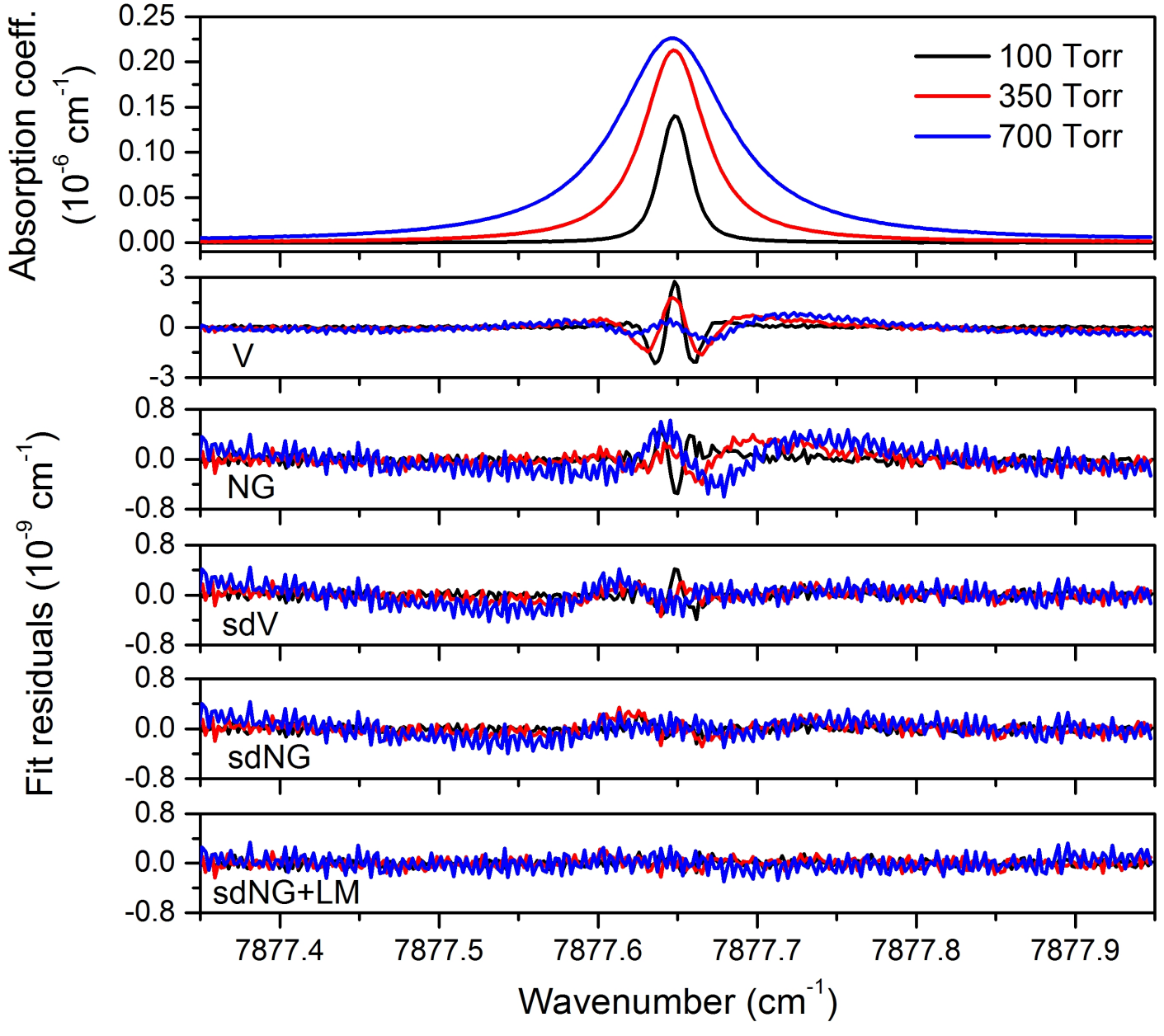
Absorption coeff. (10^{-6} cm^{-1})
0.25
0.20
0.15
0.10
0.05
0.00
100 Torr
350 Torr
700 Torr
3
0
-3
V
Fit residuals (10^{-9} cm^{-1})
0.8
0.0
-0.8
NG
sdV
sdNG
sdNG+LM
7877.4
7877.5
7877.6
7877.7
7877.8
7877.9
Wavenumber (cm^{-1})

High sensitivity spectroscopy of the O_2 band at 1.27 μm:

(II) Air-broadened line profile parameters

D. D. Tran[1], H. Tran[1,*], S. Vasilchenko[2], S. Kassi[2], A. Campargue[2], D. Mondelain[2]

Keywords: Oxygen band at 1.27 μm, Cavity ring-down spectroscopy, line intensity, line-shape, speed dependence, Dicke narrowing, line mixing, speed-dependent Nelkin-Ghatak profile, air broadening

* Corresponding author: ha.tran@lmd.jussieu.fr

Abstract:

A cavity ring down spectrometer referenced to a frequency comb is used to study the profile of air-broadened O_2 lines of the 1.27 μm band. To this aim, spectra of O_2 in dry air and of O_2 in N_2 with 2% of O_2 were measured, respectively in the 7720-7920 cm^{-1} and 7868-7887 cm^{-1} spectral ranges at room temperature and various pressures ranging from 50 to 700 Torr. Detailed line profile analysis is reported for 85 transitions using the speed dependent Nelkin-Ghatak model and a multi-spectrum treatment of the two series of spectra. Line mixing was found necessary to be taken into account in the analysis of lines in the region of the *Q* branch. The derived line parameters including the broadening and shifting coefficients, the speed dependent components of the collisional line broadening and shifting, as well as the Dicke narrowing parameter are discussed and compared to literature data. In particular, the speed dependence components of the collisional broadening are found to agree satisfactorily with predictions obtained by molecular dynamic simulations. This obtained set of line-shape parameters should allow for improved modeling of atmospheric spectra in the 1.27 μm spectral region.

1. Introduction

The atmospheric band of O_2 near 1.27 μm consists of narrow absorption lines of the $a^1\Delta_g - X^3\Sigma_g^-(0-0)$ transitions superimposed to a broad collision-induced absorption (CIA) structure. Recently this band became suitable for spaceborne observations thanks to accurate modeling of the strong mesosphere/stratosphere airglow produced by O_3 photo-dissociation [1,2]. Together with the stronger A-band near 760 nm, the 1.27 μm band is thus used to determine the air mass along the line of sight from atmospheric spectra recorded at ground by the Total Carbon Column Observing Network (TCCON) [3-5] or from space [1-3,6,7]. The derivation of the dry air column from the O_2 column is made possible by the fact that the mixing ratio of oxygen is mostly constant (20.95 %) in the Earth's atmosphere [8]. The present work is part of a project dedicated to a better characterization of this band in support of the satellite mission MicroCarb [9], dedicated to the accurate determination of column integrated concentrations of CO_2.

In a previous work, highly sensitive cavity ring down spectroscopy (CRDS) was used to determine the room temperature CIA binary coefficients from low density spectra (0.36 to 0.85 amagat) of pure oxygen and an O_2/N_2 mixture at room temperature, over the wide 7513-8466 cm^{-1} region [10]. As concerned the study of the absorption lines, a first contribution was dedicated to low pressure spectra of pure O_2 in the 7920-8085 cm^{-1} interval for pressures up to 150 Torr [11]. Compared to previous CRDS investigations [12,13], the coupling of the CRD spectrometer to a self-referenced frequency comb (SRFC) provided a much more accurate absolute frequency axis and better quality line profiles by strongly reducing the amplitude noise due to laser jitter in the flanks of the absorption lines. In addition, a higher sensitivity was achieved allowing for low pressure recordings at a few Torr, valuable for an accurate determination of the zero-pressure line centers and of the line intensities [11].

The profile of the lines of the oxygen 1.27 μm band broadened by air is of importance for atmospheric applications. This motivated a very recent line shape study of air-broadened spectra by frequency stabilized CRDS (FS-CRDS) [5]. In [14], line-shape parameters of seven air-broadenned lines of this band were obtained. Note that to the best of our knowledge, no other air-broadened line profile studies was published before for the considered band. This is due to its relative weakness (line intensities are less than 1×10^{-25} cm/molecule). As a consequence, in its present version, the HITRAN2016 database provides for the 1.27 μm band, line profile parameters transferred from the A-band [3,15] which should be validated.

It is well known that highly sensitivity recordings of the O_2 absorption lines reveal important deviations from the standard Voigt profile. As concerned the 1.27 μm band, non-Voigt effects were first observed in [16,17]. In [5], it was shown that the Voigt profile leads to large differences with the measured spectra. When the speed dependences of the collisional broadening and shifting are taken into account with the quadratic speed dependent Voigt profile (sdV), fit residuals were significantly improved. However, large fit residuals remain [5]. In [14], the speed dependent Nelkin-Ghatak (sdNG) profile, taking into account both the speed dependence and the Dicke narrowing effects, was used to fit measured spectra of 7 air-broadened O_2 lines. In this case, fit residuals were almost within the experimental noise.

Several spectroscopic studies were devoted to the A band (see [18] and references quoted therein), due to its importance for atmospheric remote sensing. In [18], the sdV profile with line mixing was adopted in the multi-spectrum fitting of the line shapes. Let us also mention the profile study of eleven lines of the B band of oxygen near 690 nm (of intensity comparable to that of the 1.27 μm band) by FS-CRDS linked to an optical frequency comb [19]. Among the various line shape models considered by Domyslawska *et al*., a better spectra reproduction was also achieved by using the sdNG profile.

In the present work, the sdNG profile with line mixing is used for a multi-spectrum treatment of two series of spectra of dry air and of a 2% mixture of O_2 in N_2. The acquisition of the spectra by CRDS referenced to a frequency comb is described in the next Section. After the description of the line profile analyses (Section 3), the retrieved line shape parameters are compared with literature in Section 4 before the concluding remarks (Section 5).

2. Experimental setup

The frequency comb referenced CRDS method and setup used for the recordings have been described in details in [20,21]. In this work, we used a set of four Distributed Feedback (DFB) laser diodes to cover the 7780-7920 cm^{-1} spectral range corresponding to most part of the considered O_2 band (see **Fig. 1**). The noise equivalent absorption, α_{min}, of the recordings was between 7×10^{-11} cm^{-1} and 2.5×10^{-10} cm^{-1} depending on the diode. Two series of spectra were recorded: *(i)* the first one (named dry air hereafter) using a mixture of O_2 and N_2 with an O_2 relative concentration of 20.95±0.06% (Air Liquide; O_2+N_2>99.9999%) with total pressures between 50 and 700 Torr and *(ii)* a second one (**Fig. 2**) (named 2% mixture below) with 2.00±0.02% of O_2 in N_2 (OXY-105 from Air Liquide) with total pressure between 100 and 700 Torr. The latter mixture was specifically dedicated to measurements of the strong *Q* branch lines which are too strong to be measured with dry air at high pressure. The pressure inside the

high-finesse cavity (HFC) was continuously monitored using a 1000 mbar pressure gauge (Model 622 Barocel pressure sensor from Edwards, 0.15% accuracy of the reading) and was regulated with a solenoid valve and a proportional integral software based loop. The HFC temperatures, included in **Table 1,** were measured with a temperature sensor (TSic 501, IST-AG, ±0.1 K accuracy) fixed on the cell surface, covered by an external blanket for thermal isolation.

O_2 conc. in N_2 (%)	**Total pressure (Torr)**	**Temperature (K)**	**Spectral range (cm^{-1})**
20.95±0.06	49.7 - 50.7	294.6 - 295.3	7783.69 - 7915.91
	99.8 - 100.2	294.4 - 295.3	
	199.6 - 200.3	294.4 - 295.2	
	299.4 - 300.1	294.1 - 295.3	
	499.4 - 500.1	294.1 - 295.3	
	699.2 - 700.0	294.6 - 295.1	
2.00±0.02	99.7 - 100.1	294.5 - 295.3	7868.30 - 7886.65
	199.7 - 200.2	294.5 - 295.4	
	349.5 - 350.2	294.5 - 295.4	
	499.4 - 500.3	294.5 - 295.5	
	699.2 - 700.1	294.6 - 295.4	

Table 1: Pressure, temperature and concentration conditions of the recordings. For the pressure and temperature, the minimum and maximum are reported taking into account the fact that, for a given pressure, the different parts of the spectrum were recorded at different days.

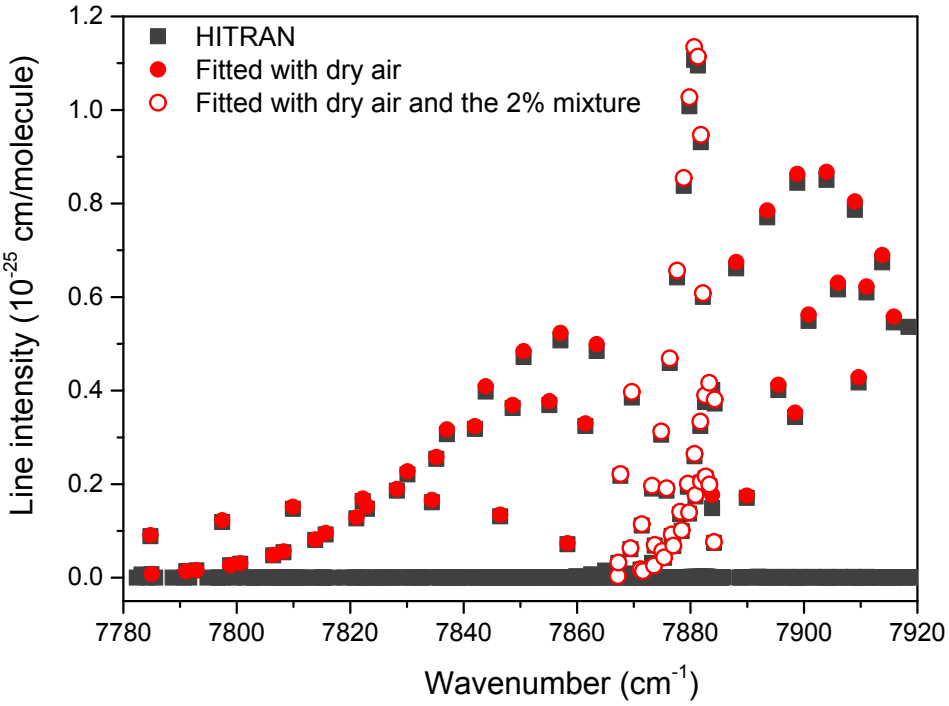

Figure 1. Overview of the O_2 transitions of the $\boldsymbol{a^1\Delta_g - X^3\Sigma_g^-(0-0)}$ band analyzed in this work: in red full circles are lines analyzed using dry air while in red open circles are those measured using both dry air and the 2% mixture. The black symbols correspond to the HITRAN line list [22].

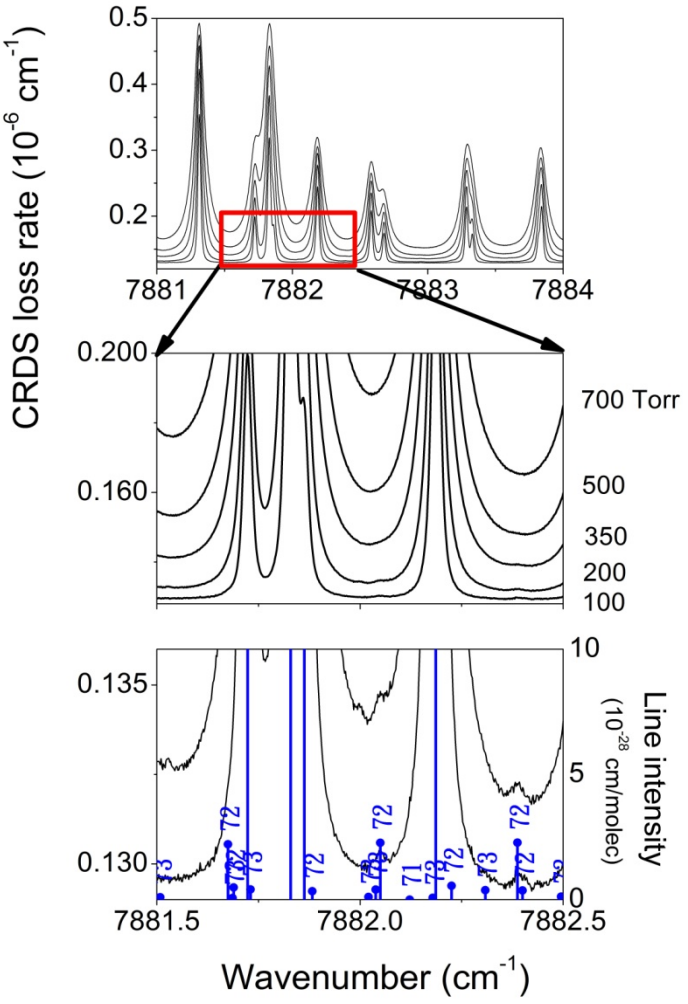

Figure 2. Part of the Q-branch recorded with the 2% mixture of O_2 in N_2 at different pressures between 100 and 700 Torr (Upper panel). Two successive zooms are shown in the middle and lower panels. Line intensities provided by the HITRAN2016 database are also plotted on the lower panel showing that weak lines of the $^{16}O^{18}O$ isotopologue (identified by 72 in HITRAN) are observed thanks to a minimum detectable absorption coefficient of 6.5×10^{-11} cm^{-1}. Note the increase of the baseline level due to the CIA.

The overview of the 85 lines analyzed in this work is presented in **Figure 1.** They all correspond to magnetic dipole transitions of the main isotopologue, $^{16}O_2$, and have intensity larger than 3.5×10^{-28} cm/molecule.

3. Analysis procedure

The measured spectra were analyzed using a multi-fitting code developed previously by some authors of this paper [23,24]. Parameters of lines with intensity greater than 3.5×10^{-28} cm/molecule were adjusted while contribution of the lines of lower intensity were calculated using data provided in the HITRAN 2016 database [22] and fixed in the fitting procedure (this is for instance the case of the lines of the $^{16}O^{18}O$ minor isotopologue showed in **Fig. 2**). As mentioned above, the air-broadened spectra of the strong lines in the *Q* branch could not be

recorded with the air sample for the highest pressure values. Among the 83 analyzed air-broadened lines, 41 were recorded with the 2% mixture and simultaneously considered in the multi-spectrum treatment.

Line profile fittings were performed with various line-shape models: the usual Voigt profile, the Nelkin-Ghatak (NG) profile [25] taking the Dicke narrowing effect into account, the (quadratic) speed dependent Voigt (sdV) profile [26,27], the (quadratic) speed dependent Nelkin-Ghatak (sdNG) and the Hartmann-Tran (HT) [28,29] profiles. Except for the *Q* branch lines, the sdNG profile, taking into account both the Dicke narrowing effect and the speed dependences of the line width and shift leads to the best line shape reproduction, the fit residuals being almost at the experimental level (see **Fig. 3**). With respect to the sdNG profile, the HT model has another parameter (the correlation between velocity changes and internal state changes collisions) to be fitted but it leads to very similar fit residuals as the sdNG profile. The latter was thus adopted for the analysis. For *Q* branch lines, line-mixing (LM) effect is also taken into account using the first-order approximation of [30]. Within this model, the spectral shape of a transition at wavenumber σ is given by ([28] and references therein):

$$I(\sigma) = \frac{1}{\pi} Re[(1 + iY)F(\sigma)]. \quad (1)$$

Where $Y = P\zeta$ is the first-order line-mixing parameter and ζ is the line-mixing pressure-normalized coefficient (in atm^{-1}), which accounts for the coupling between the considered line and the others. The normalized line-shape quantity $F(\sigma)$ is function of seven parameters, *i.e.* $F(\sigma) = f(\sigma - \sigma_0, \Gamma_D, \Gamma_0, \Gamma_2, \Delta_0, \Delta_2, \nu_{vc})$. σ_0 is the unperturbed position of the line and Γ_D the Doppler broadening half-width. The speed dependent collisional half-width and -shift are modeled using the quadratic law [26,27], *i.e.* $\Gamma(v) + i\Delta(v) = \Gamma_0 + i\Delta_0 + (\Gamma_2 + i\Delta_2)\left[\left(v/\tilde{v}\right)^2 - 3/2\right]$ in which $\tilde{v} = \sqrt{2k_BT/m}$ is the most probable speed for an absorbing molecule of mass m. Γ_0 and Δ_0 are thus the speed-averaged collisional width and shift while Γ_2 and Δ_2 represent the speed dependent components of $\Gamma(v)$ and $\Delta(v)$, respectively. Finally, ν_{vc} is the Dicke narrowing parameter or the rate of velocity changing (VC) collisions, modeled through the hard collision approximation [25,31]. Γ_0, Γ_2, Δ_0, Δ_2 and ν_{vc} are proportional to the total pressure *P* while σ_0 is constant with *P*.

In the fitting procedure, the line position σ_0 was fixed to values of Ref. [11] derived by high sensitivity CRDS spectra of pure O_2 measured at low pressure. The Doppler line broadening half-width, Γ_D, was also fixed to the value calculated from the measured

temperature. Since lines are quite isolated (see **Fig. 1**), a spectral range of about 1 to 2 cm^{-1} was considered at a time, in order to simplify the fitting procedure and to minimize the influence of the contribution of the CIA [10]. The contribution of lines close to the considered spectral region ($\pm$ 1 cm^{-1} from the center of the considered line) was nevertheless taken into account using HITRAN2016 and fixed in the fitting procedure. For each considered spectral interval and each pressure, a linear baseline [i.e. $a + b(\sigma - \sigma_0)$] was adjusted. The pressure and temperature were calculated as the average pressure and temperature over the considered spectral interval. Note that, the variation of pressure and temperature was very small (*i.e.* about 0.07 Torr and 0.04 K over 1 cm^{-1}), this averaging has no consequences for the fit residuals and the values of the retrieved line parameters. For each line, the line-shape parameters were constrained to be proportional to the total pressure (*i.e.* $\gamma_0 = \frac{\Gamma_0}{P}, \gamma_2 = \frac{\Gamma_2}{P}, \delta_0 = \frac{\Delta_0}{P}, \delta_2 = \frac{\Delta_2}{P}, \beta = \frac{\nu_{vc}}{P}$ and $\zeta = \frac{Y}{P}$ where γ_0, γ_2, δ_0, δ_2, β and ζ are constant with pressure) while the line area was fitted individually for each pressure. The line intensity was then obtained as the slope of the linear fit of the line area with the partial pressure of O_2.

Figure 3 presents an example of fit residuals obtained with various line-shape models for the P7P7 air-broadened line at three pressures. The Voigt profile leads to large fit residuals, especially at low pressure. When velocity changes are taken into account by using the Nelkin-Ghatak profile, residuals are decreased by a factor of about 3. Better residuals are obtained with the sdV profile showing that speed dependence effects have more impact than velocity changes effect in the considered pressure range. Finally, the sdNG and the HT profiles, taking into account both velocity and speed dependence effects give very similar fit residuals, both mostly within the experimental noise.

For the *Q* branch, since lines are overlapping at the considered pressure conditions, line-mixing effects must be taken into account. This was done here by using the first-order approximation [see Eq. (1)]. The influence of line-mixing effects is illustrated in **Fig. 4**. The inclusion of the line-mixing allows for a significant reduction of the residuals practically to the noise level.

No line-mixing effect is observed for the *P* and *R* lines. The sdNG profile together with the first-order line-mixing was thus retained for the analysis of most of the considered *Q* lines while, the sdNG profile was found sufficient for the *P* and *R* lines. As recordings with dry air and with the 2% mixture were used in the *Q*-branch region, line-shape parameters for self- and N_2-broadened O_2 could be retrieved in this region while only air-broadened line-shape

parameters were determined in the *P* and *R* regions. The retrieved line intensity and line shape parameters are presented and discussed in the next section.

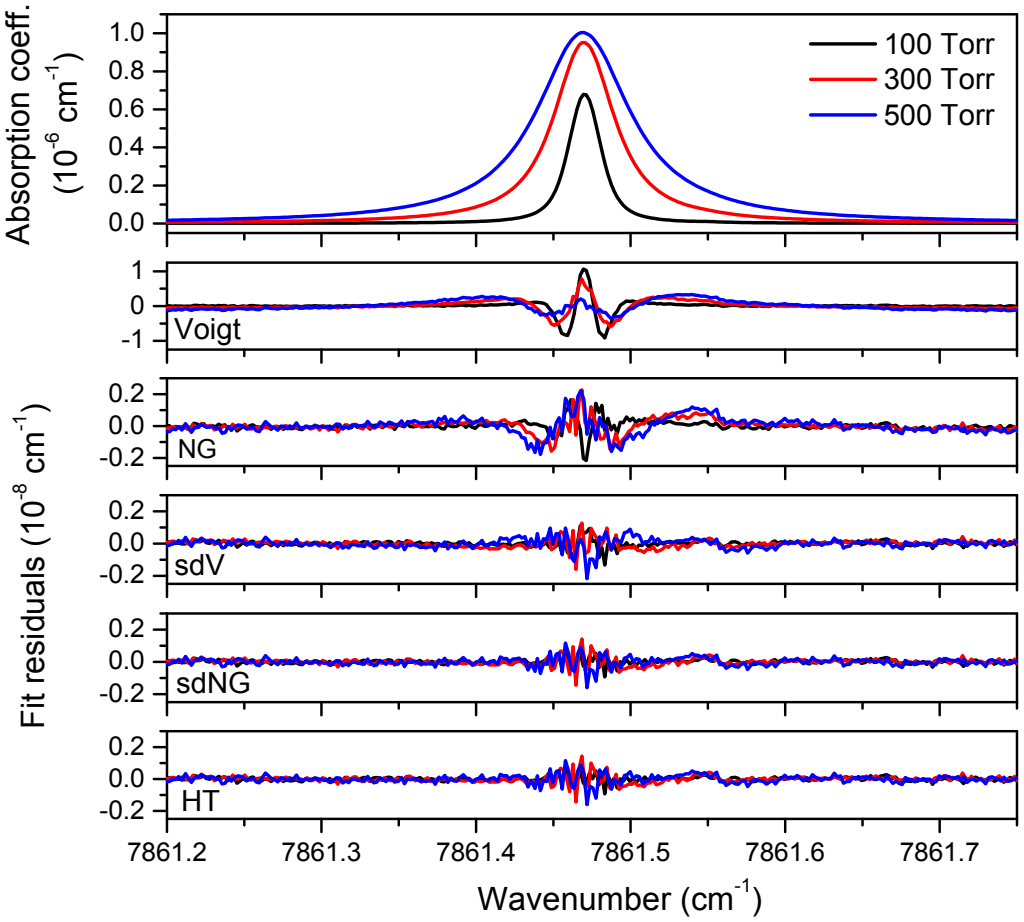

Figure 3. Spectra of the P7P7 line of O_2 broadened by air (top panel) measured by CRDS at three pressures. The lower panels represent the multi-fit residuals obtained with the Voigt (V), the Nelkin-Ghatak (NG), the quadratic speed dependent Voigt (qsdV), the quadratic speed dependent Nelkin-Ghatak (qsdNG) and the Hartmann-Tran (HT) profiles, respectively. Note the different scale adopted for the Voigt residuals.

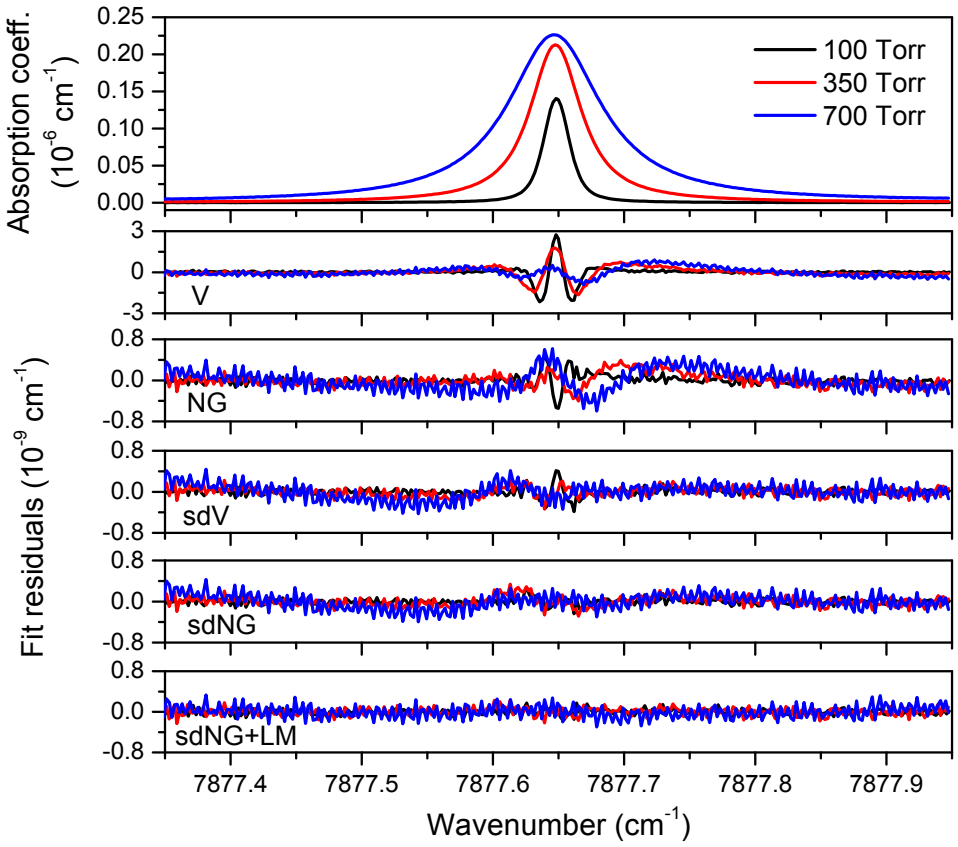

Figure 4. Spectra of the Q15Q15 line (top panel) measured by CRDS at three pressures for 2% of O_2 in N_2. The lower panels show the multi-fit residuals obtained with the Voigt (V), Nelkin-Ghatak (NG), speed dependent Voigt (sdV), speed dependent Nelkin-Ghatak (sdNG) profiles and the speed dependent Nelkin-Ghatak profile together with line-mixing. Note the different scale adopted for the Voigt residuals.

4. Retrieved line parameters and comparisons with previous data

4.1 Line intensity

For each considered transition, the line area was retrieved individually from each pressure and at the temperature of the measurement. This line surface was then converted to the corresponding value at 296 K using the lower energy level of the considered transition as provided by the HITRAN database [22]. The integrated line intensity at 296 K was then obtained from the slope of the linear fit of the line area *versus* O_2 partial pressure. **Figure 5** shows four examples of the retrieved line surfaces *versus* the O_2 partial pressure and their linear fits. For most of the considered *P* and *R* lines, line intensity was obtained from spectra at 5 or 6 pressures while for the *Q* lines, up to 10 or 11 pressure values were used. For some intense *Q* lines, the too saturated spectra were excluded in the intensity determination. The obtained values of the line intensities as well as the standard deviations of the linear fit are listed in **Table 2**.

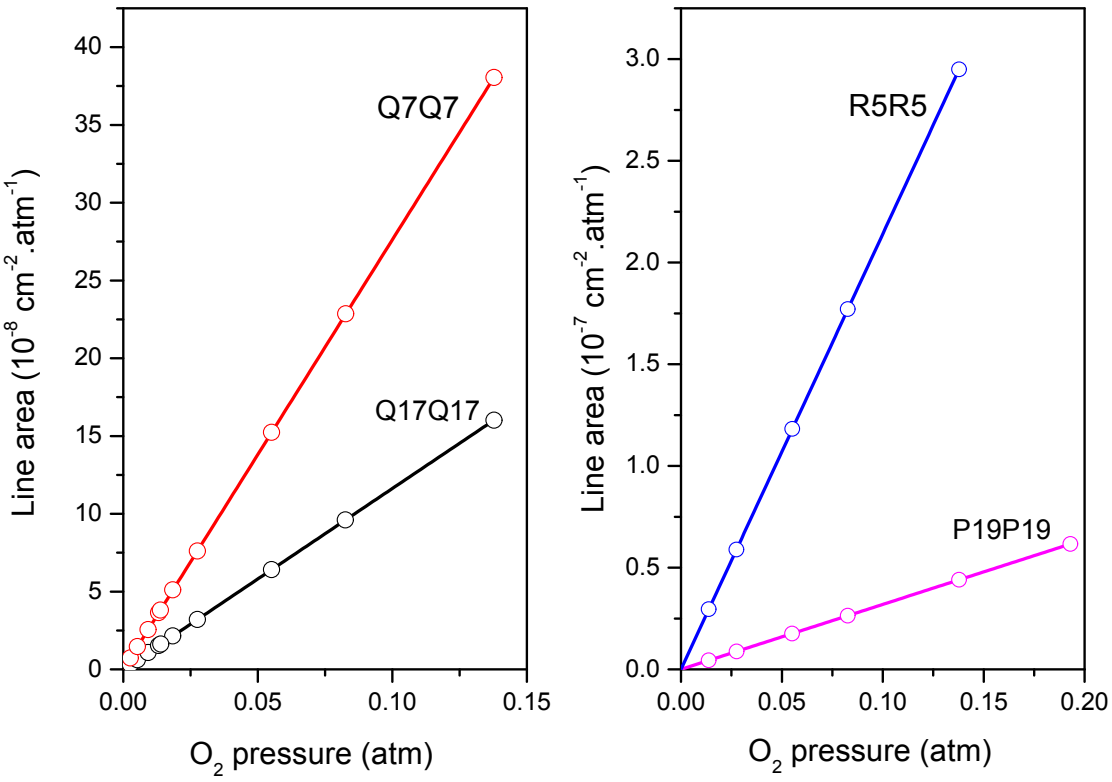

Figure 5. Example of the pressure dependences of line areas and corresponding linear fits leading to the line intensity.

The retrieved line intensity was first compared to values provided by the HITRAN database [22]. HITRAN line intensities of the considered magnetic dipole transitions were calculated by Orr-Ewing on the basis of FTS intensities measured in Ref. [32]. The ratios of the line intensities obtained in this work over HITRAN values are displayed on the left-hand panel of **Fig. 6.** HITRAN values are found significantly overestimated by 1 to 4 % and clear systematic deviations depending on the considered branch are evidenced. Comparison with intensities derived in the recent works of [5] and [11] was performed. In [5], spectra of O_2 in air were measured at room temperature for three pressure conditions (495, 745 and 982 Torr). The spectroscopic parameters including line intensity were obtained from fits of the measured spectra with the quadratic speed dependent Voigt profile. In [11] the pure O_2 spectra at low pressure was studied with the same CRDS setup used in the present study and the sdNG profile was used to model the measured line shape. In the right-hand panel of **Fig. 6**, we present the intensity ratios of our values compared to [5] and [11]. The agreement with [5] and [11] is much better than with HITRAN2016. Nevertheless, between 7860 cm^{-1} and 7890 cm^{-1} the dispersion of the plotted ratio is larger than for the rest of the studied spectral range. This region includes

strong and very dense absorption lines, partially saturated in dry air spectra, which may explain the observed deviation. Furthermore, this region corresponds to the spectral interval where the 2% mixture spectra were used, the origin of the observed intensity differences might be related to the impact of the 1% uncertainty on the stated O_2 relative concentration in the 2% mixture (see **Table 1**).

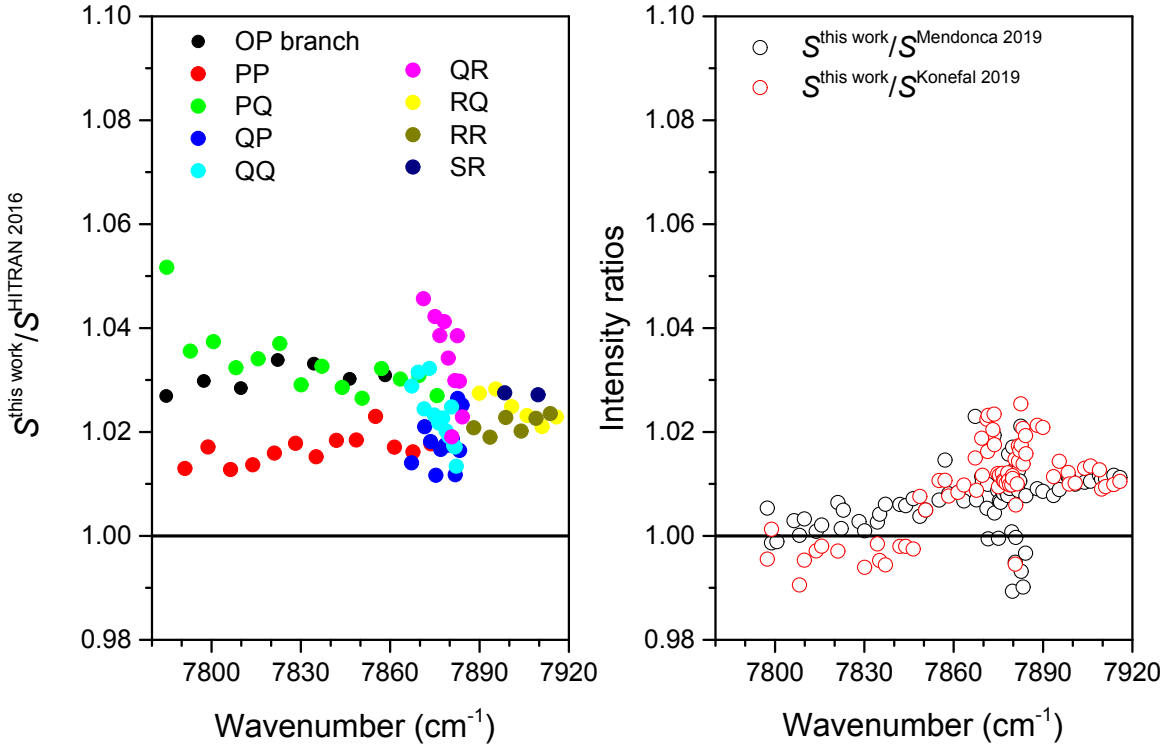

Figure 6. Ratios of line intensities obtained from this work and those from HITRAN2016 [22] (left side) as well as those of Refs. [11] and [5] (right side). In [11] and [5], the sdNG and sdV profiles respectively were used to model the measured spectral shapes.

4.2 Pressure-broadening and -shifting parameters

For the lines analyzed using both air and 2% mixture spectra, the self-broadening and N_2-broadening contributions could be retrieved separately. For instance, the line-broadening coefficient in both mixtures can be expressed as $\gamma_0 = x_{O_2}\gamma_0^{O_2} + x_{N_2}\gamma_0^{N_2}$, where x_{O_2} and $x_{N_2}$are the relative concentrations of O_2 and N_2, respectively. $\gamma_0^{O_2}$and $\gamma_0^{N_2}$ are the corresponding self- and N_2-broadening coefficients, which could be both determined in the Q branch region. Conversely, only the air-broadening coefficient of the mixture γ_0 could be determined in the P and R branches were only air-broadened spectra were used.

In **Figure 7**, the retrieved values for the O_2- and N_2-broadening $\gamma_0^{O_2}$ and $\gamma_0^{N_2}$ (left) and -shifting $\delta_0^{O_2}$ and $\delta_0^{N_2}$ (right) are plotted as a function of the rotational momentum quantum number, N'', of the lower level of the transition. The estimated uncertainties (twice the standard deviation obtained from the fits) are also presented. The results show that the O_2- and N_2-broadening coefficients are very close to each other while large differences are noted for the pressure shifts. This observation was also reported in [11] in which the measured self-broadening and shifting coefficients were compared to those of O_2 in air in HITRAN and in [5]. The self-broadening and -shifting coefficients, corresponding to an empirical rotational dependence obtained in [11] are also included in **Fig. 7** for comparison. For $\gamma_0^{O_2}$, this analytical function is in very good agreement with our measured values except for low N''. For $\delta_0^{O_2}$, the empirical linear dependence of [11] is found slightly higher than the average value of our measurements. Let us note the larger dispersion for the measured $\delta_0^{O_2}$ values with respect to $\delta_0^{N_2}$. This is due to the small self-broadening contribution in the 2% mixture, the O_2/air spectra for these lines being almost all saturated. Finally, the corresponding air-broadening and shifting parameters were calculated using $\gamma_0^{air} = 0.21\gamma_0^{O_2} + 0.79\gamma_0^{N_2}$ and $\delta_0^{air} = 0.21\delta_0^{O_2} + 0.79\delta_0^{N_2}$.

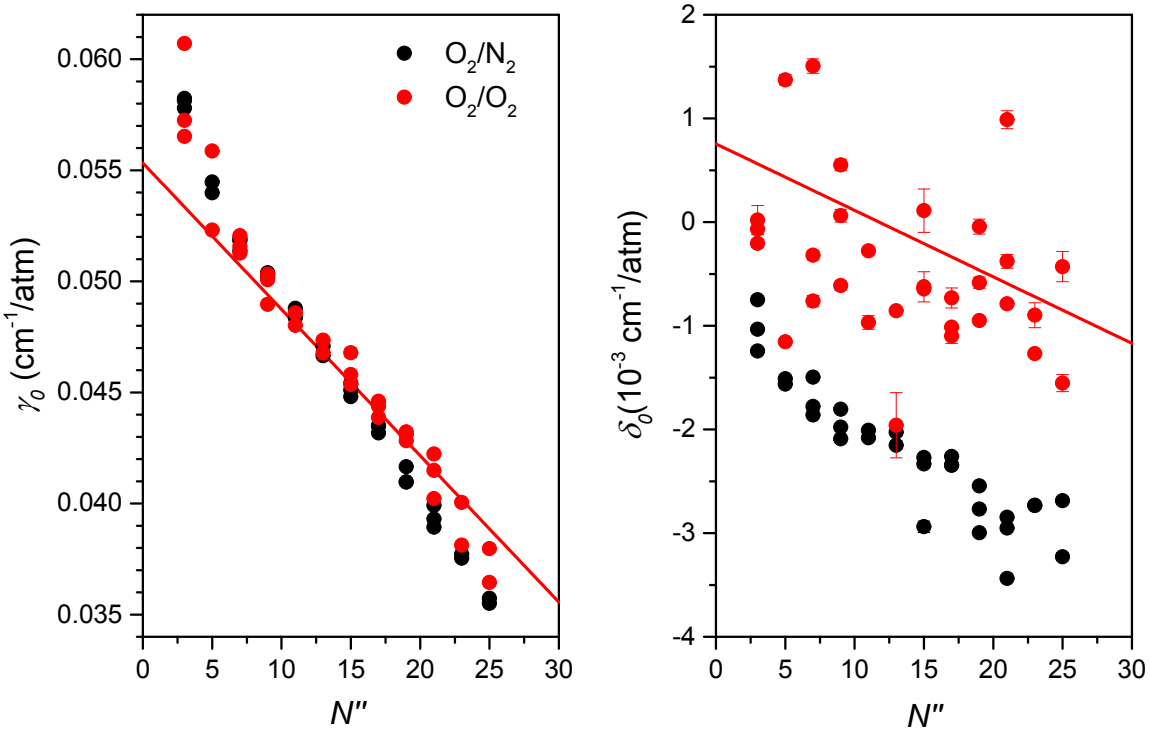

Figure 7. N_2 and O_2 line-broadening and -shifting coefficients for Q branch lines, deduced from multi-fitting the spectra measured with the two mixtures under various pressure conditions (see Table 1). The red straight lines are calculated from the empirical rotational dependences for γ_0 and δ_0 proposed in [11].

The obtained γ_0^{air} values gathered with values derived for the lines recorded only in air are presented in **Fig. 8**. The obtained dataset is compared with those provided in HITRAN2016 and measured by [5] in the left- and right-hand panel, respectively. The sources of HITRAN air-broadening coefficients of the considered 1.27 µm band are [15] and [3] and are thus related to the A-band. In [15], O_2- and N_2-broadening coefficients were retrieved from a series of FTS laboratory spectra. In [3], to better reproduce FTS atmospheric spectra in the 1.27 µm, Washenfelder *et al.* increased by 1.5% the values from [33] in which air-broadening coefficients were represented by an analytical function, adjusted on measured values (see [33] and references therein). As illustrated in **Fig. 8**, our values are slightly larger than HITRAN values with an average relative difference of 2.1(±1.3)%. A much better agreement is observed with [5], the average relative difference being 0.4(±1.0)%.

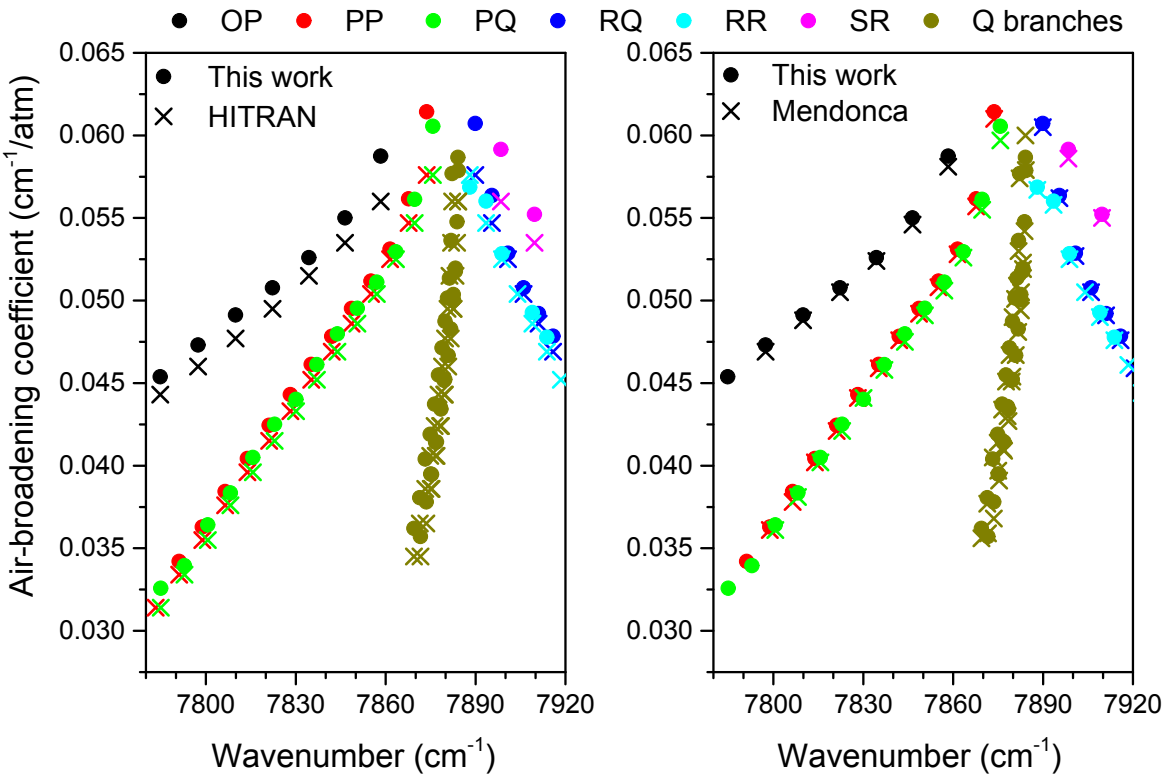

Figure 8. Comparison between the air-broadening coefficients.
Left panel: Present results (full circles) compared to HITRAN (crosses)
Right panel: Present results (full circles) compared to [5] (crosses)
Data are plotted versus the line position to clearly distinguish the different branches.

The obtained air-pressure shifting coefficients, δ_0^{air}, are compared with those of

HITRAN2016 and [5] in the left- and right-hand panels of **Fig. 9**, respectively. HITRAN values from [3], thus related to the A band, have a significantly larger magnitude than those obtained in this work. A much better agreement is obtained when compared to [5]. However, our values remain smaller in amplitude than those of [5] (see right panel of **Figure 9**). This may be related to the differences in the zero-pressure line centers. In the present work, the zero-pressure positions were constrained to very accurate values (uncertainty less than 3×10^{-5} cm^{-1}) reported in [11] from low pressure (5 Torr) CRDS spectra referenced to a self-referenced frequency comb. Apparently, Mendonca *et al.* did not determine the zero-pressure positions from their FS-CRDS spectra [the used setup was not referenced to a frequency comb and only relatively high pressure spectra (i.e. 495, 745 and 982 Torr) were recorded]. As illustrated in Fig. 9 of [11], the zero-pressure values adopted by Mendonca *et al.* coincide with HITRAN values increased by a constant value of 6.82×10^{-4} cm^{-1} leading to differences between 5×10^{-4} cm^{-1} and 7×10^{-4} cm^{-1} compared to [11]. Therefore, if using the line positions of [11], the magnitude of δ_0^{air} retrieved from the measured spectra of [5] should be much smaller, thus closer to our values. Note also that the observed difference for the air-pressure shift between [5] and our work cannot be explained by the difference in the used line-shape (a qsdV profile was used in [5] while a qsdNG profile is used here). In fact, several studies (e.g. [19,24,34]) have shown that these two profiles lead to very similar pressure shifting coefficients.

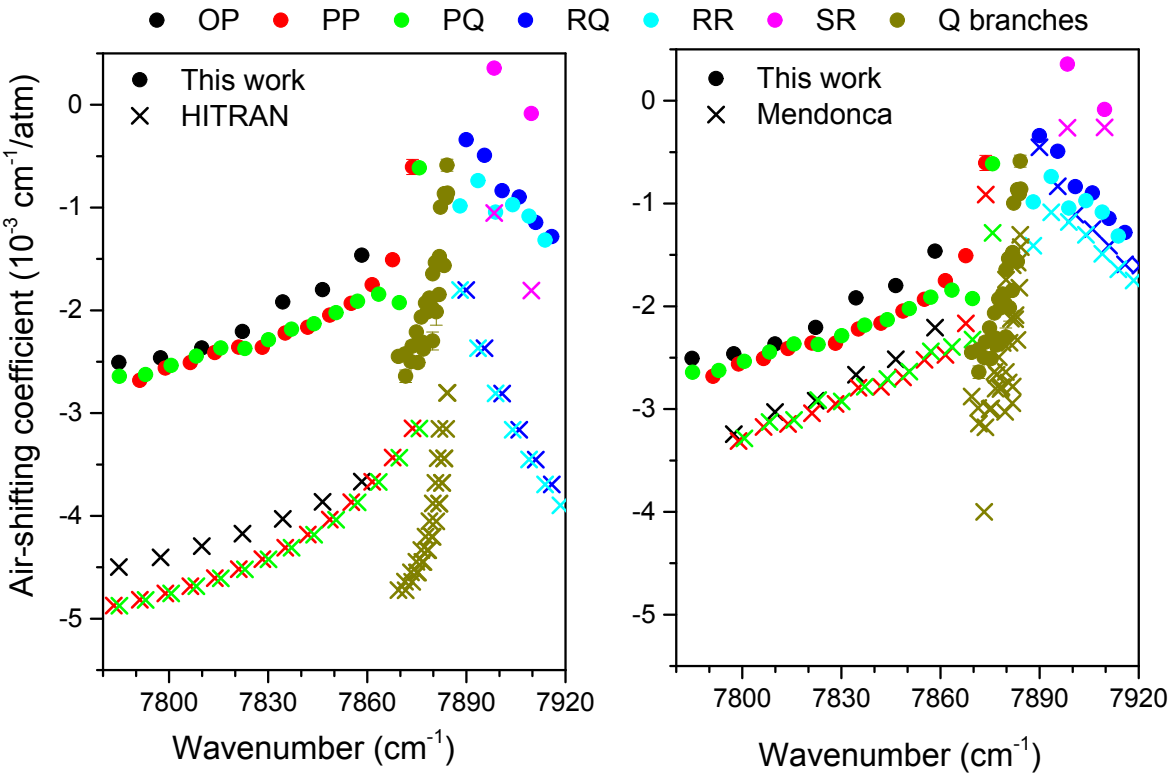

Figure 9. Comparison between the air-pressure shifting coefficients.
Left panel: Present results (full circles) compared to HITRAN (crosses)
Right panel: Present results (full circles) compared to [5] (crosses)
Data are plotted versus the line position to clearly distinguish the different branches.

4.3. The high-order line-shape parameters

The speed dependent components, γ_2 and δ_2, of the collisional line broadening and shifting are plotted in **Fig. 10** *versus* N'' and compared with values obtained from [5]. No branch dependence as in the case of γ_0 and δ_0 is observed. All the obtained data are therefore presented by the same color code. The δ_2 values are associated with large uncertainty and have a strong dispersion with no observable rotational dependence. For the speed dependence of the line broadening, the γ_2/γ_0 ratio is plotted instead of γ_2. This ratio increases with increasing N'' value. This behavior is also observed with values of [5]. However, our values are significantly smaller than those of [5]. This is probably due to the used line-shape models, the sdV usually leading to larger γ_2/γ_0 values, (see e.g. [24,34,35]). The γ_2/γ_0 values are also compared with the theoretically predicted values of [14]. In the latter, spectra of air-broadened O_2 were simulated using molecular dynamic simulations (MDS). Line-shape parameters were then deduced from fits of the MDS-calculated spectra with the qsdNG profile. Since there are no vibrational and electronic dependences in these MDS, the pressure shift cannot be predicted and no spin dependence could be considered. The predicted line-shape parameters are band- and branch-independent [14]. A good agreement between our values and those of [14] is observed confirming the interest of the predictions which have the advantage to be easily performed for various pressure and temperature conditions. The measured values of [14], obtained from fits of spectra of seven O_2 lines using the qsdNG profile are also plotted in the left part of **Fig. 10** showing good agreement with our values. For air-broadened O_2, the qsdNG profile was used to model the line shape in [36] for the P9P9 line of the B band. The obtained values for the speed dependent broadening and shifting are plotted in **Fig. 10**. The good agreement between these values and our values show that we can safely assume that these high-order line-shape parameters are band-independent for O_2.

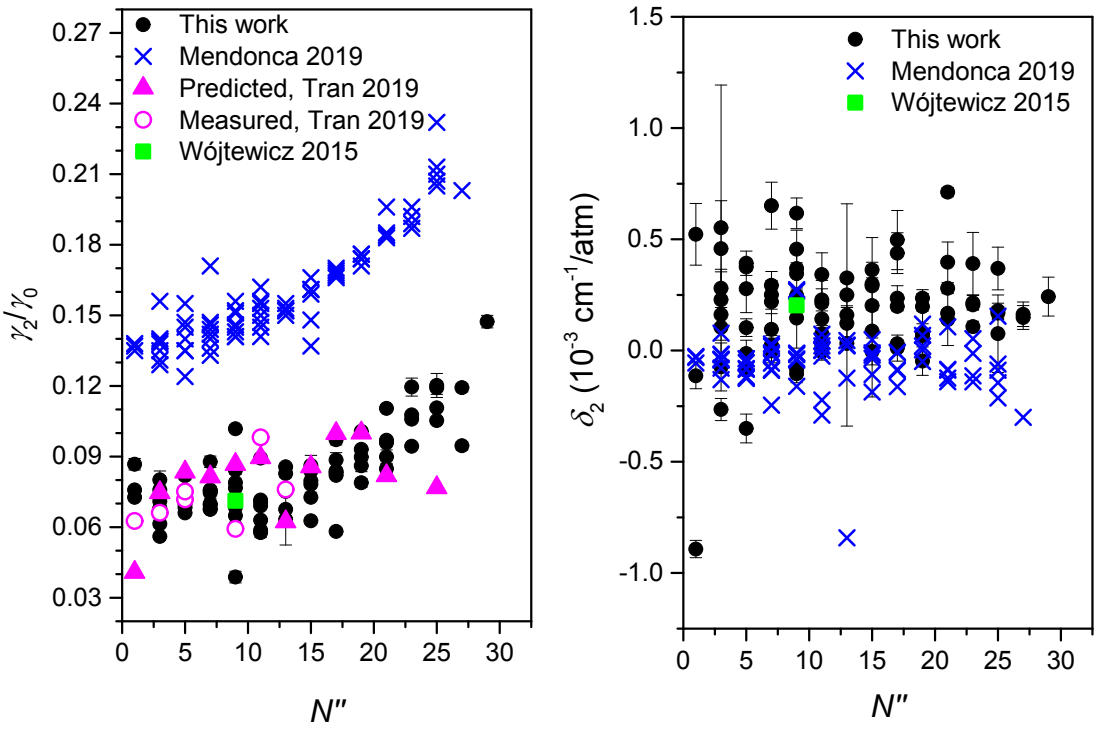

Figure 10. The speed-dependent components of the collisional broadening and shifting for O_2 in air versus the angular momentum quantum number N" of the lower level of the transition. In full circles are values obtained in this work while in crosses are results of Ref. [5]. Magenta triangles and open circles are respectively the theoretically predicted and measured values obtained in [14]. Green full squares are results of [36] for the P9P9 line of the B band.

The retrieved Dicke narrowing coefficients are shown in the left part of **Fig. 11**. These values are also compared with the predictions as well as values retrieved from measured spectra of [14] showing a rather good agreement. Both the measured and predicted values increase with increasing values of N''. It is well known that the β value strongly depends on the line-shape model chosen to fit the measured spectra. Therefore, no comparison with values obtained with other profiles (*e.g.* the Galatry profile used in [37,38], the Nelkin-Ghatak profile used in [18] for the A band spectra, the Galatry and NG profiles in [36] for the B band) is shown here. The unique sdNG value of [36] for the P9P9 line of the B band is also plotted in **Fig. 11** for comparison.

In the right part of **Fig. 11** are shown the first-order line-mixing coefficients retrieved from the measured Q lines. To the best of our knowledge, there is no measured or calculated values of line-mixing coefficients in this band so far. Several studies are devoted to the calculations and/or measurements of line-mixing effects in the more intense A band (see [18] and references therein). Since the structure of the band is completely different [39], comparison with line-mixing parameters obtained for the A band is thus meaningless.

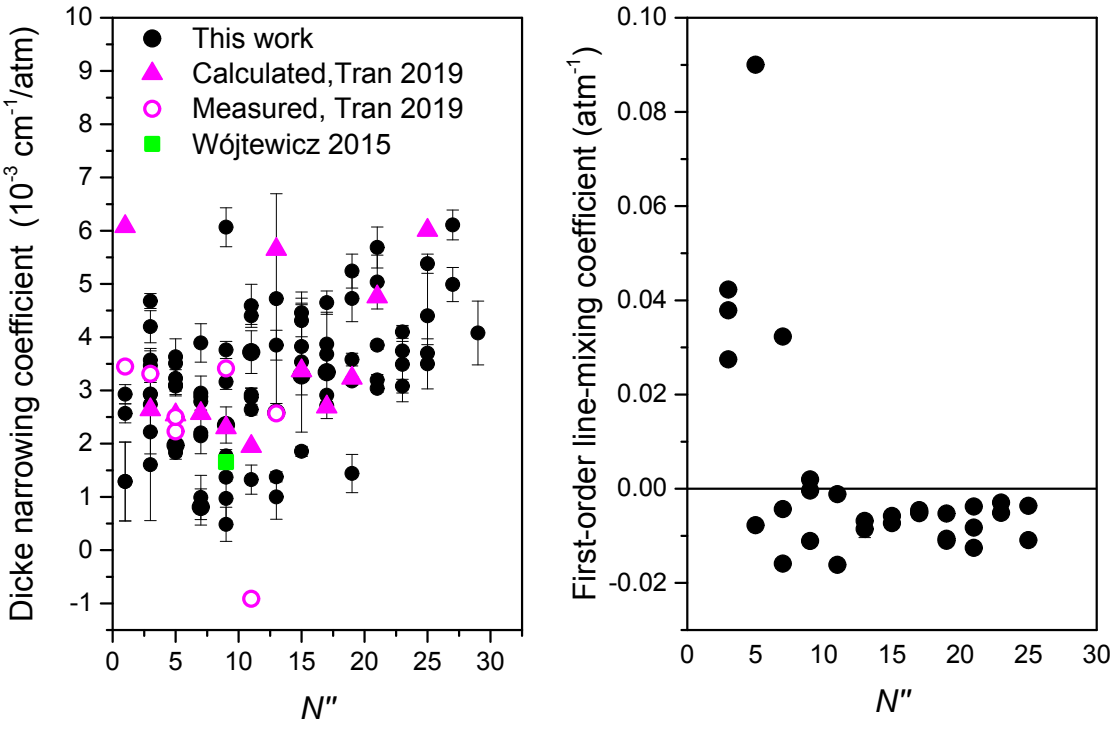

Figure 11. Left panel: The retrieved Dicke narrowing coefficients for O_2 in air vs the angular momentum quantum number N" of the lower level of the transition. Magenta triangles are the theoretically predicted values obtained in [14]. Green full square is result of [36] for the P9P9 line of the B band. Right panel: The first-order line-mixing parameter for O_2 in air, retrieved from the measured Q lines

5. Discussions and conclusion

Line-shape parameters of more than eighty lines of O_2 broadened by air in the 1.27 μm band were obtained for the first time with the quadratic speed dependent Nelkin-Ghatak profile. High sensitivity spectra of these transitions were measured with a frequency comb referenced cavity ring down spectrometer with dry air and with a 2% O_2/N_2 mixture. The pressure condition of the measurement covered a large range, from 50 to 700 Torr. Thanks to the high signal to noise ratio of the measurements and the large pressure range considered, refined effects such as the speed dependences of the collisional broadening, the Dicke narrowing and the collisional line mixing were evidenced. The use of the sdNG profile and the first-order line mixing allows to model all the measured line shapes at almost the experimental noise. The obtained data were compared with those provided in the HITRAN database showing several differences, for both line intensity, line broadening and line shifting coefficients. Comparison with the recent work of [5] for this band, reveals that the magnitude of the air-pressure shifting coefficients of [5] is overestimated. It also shows that the used line-shape model leads to much better agreement with measured spectra than the usual Voigt but also the speed dependent Voigt profile, used in [5]. The line-shape parameters obtained in this work should allow for improvement in the modeling of atmospheric observations in the 1.27 μm spectral region. In addition, comparison between the obtained high-order line-shape parameters with the predictions by molecular dynamic simulations [14] shows very good agreement, confirming the interest of the latter. Such predictions can be made for various pressure and temperature conditions, thus could be a powerful tool for providing accurate line-shape parameters for

spectroscopic databases and applications.

Table 2 : Line intensity and air-broadened line-shape parameters of the 85 O_2 lines in the 1.27 μm band, analyzed in this work. Line position is taken from [11] and line identification from the HITRAN database. γ_0 is in cm^{-1}/atm while δ_0, γ_2, δ_2 and β are in 10^{-3} cm^{-1}/atm and the first order line-mixing coefficient ζ is in 10^{-3} atm^{-1}. The corresponding uncertainty (unc, see text) for each parameter is in the unit of the last quoted digit. For lines for which the line position is denoted with a "*", the high-order line-shape parameters are considered as outliers.

σ_0 (cm^{-1})	line	S (cm/molecule)	unc	γ_0	unc	δ_0	unc	γ_2	unc	δ_2	unc	β	unc	ζ	unc
7784.797157	O17 P16	9.0986E-27	35	0.04538	2	-2.51	1	3.72	2	0.20	2	3.34	8	0.00	0
7784.981886	P29 Q28	7.8992E-28	110	0.03258	4	-2.64	3	4.80	8	0.24	9	4.08	60	0.00	0
7791.115122	P27 P27	1.4050E-27	7	0.03420	2	-2.68	2	4.08	6	0.15	5	4.99	32	0.00	0
7792.885254	P27 Q26	1.5958E-27	10	0.03395	2	-2.63	2	3.21	6	0.16	6	6.11	28	0.00	0
7797.419013	O15 P14	1.2265E-26	4	0.04731	2	-2.46	1	3.70	2	0.29	1	3.28	8	0.00	0
7798.845848	P25 P25	2.6964E-27	12	0.03629	2	-2.56	1	3.82	4	0.18	3	5.38	18	0.00	0
7800.633630	P25 Q24	3.0966E-27	11	0.03641	2	-2.54	1	4.03	2	0.17	3	3.70	16	0.00	0
7806.421850	P23 P23	4.8441E-27	4	0.03844	2	-2.51	1	4.07	2	0.21	2	4.10	12	0.00	0
7808.227444	P23 Q22	5.6006E-27	18	0.03835	2	-2.45	1	3.62	4	0.21	3	3.74	18	0.00	0
7809.894157	O13 P12	1.5149E-26	2	0.04913	2	-2.37	1	3.69	2	0.33	2	2.58	8	0.00	0
7813.843390	P21 P21	8.1672E-27	21	0.04044	2	-2.41	1	3.92	2	0.28	2	3.85	8	0.00	0
7815.667023	P21 Q20	9.5600E-27	12	0.04050	2	-2.37	1	3.88	2	0.17	1	3.04	8	0.00	0
7821.110628	P19 P19	1.2882E-26	2	0.04244	2	-2.36	1	3.95	2	0.23	2	3.58	12	0.00	0
7822.221867	O11 P10	1.6924E-26	7	0.05077	2	-2.21	2	2.98	10	0.34	10	3.72	40	0.00	0
7822.952610	P19 Q18	1.5275E-26	2	0.04251	2	-2.37	2	4.28	6	-0.05	6	1.44	36	0.00	0
7828.223646	P17 P17	1.8952E-26	7	0.04430	2	-2.36	2	3.68	6	0.24	6	3.68	24	0.00	0

7830.084392	P17 Q16	2.2722E-26	27	0.04402	2	-2.29	2	2.56	6	0.01	6	4.65	22	0.00	0
7834.401709	O 9 P 8	1.6644E-26	5	0.05260	2	-1.92	2	3.41	6	0.62	7	2.35	34	0.00	0
7835.182401	P15 P15	2.5807E-26	14	0.04613	2	-2.22	1	3.35	4	0.36	4	4.46	18	0.00	0
7837.062488	P15 Q14	3.1692E-26	24	0.04612	2	-2.18	1	2.89	6	-0.00	6	4.31	30	0.00	0
7841.986766	P13 P13	3.2395E-26	32	0.04783	2	-2.16	1	3.23	6	0.25	6	3.85	28	0.00	0
7843.887027	P13 Q12	4.0937E-26	51	0.04798	2	-2.13	2	3.97	8	0.12	8	1.00	42	0.00	0
7846.434323	O 7 P 6	1.3496E-26	4	0.05501	2	-1.80	2	4.15	6	0.25	6	0.81	34	0.00	0
7848.636466	P11 P11	3.6939E-26	9	0.04952	2	-2.05	1	3.50	4	0.14	5	2.87	18	0.00	0
7850.558213	P11 Q10	4.8440E-26	13	0.04953	2	-2.02	1	3.42	2	-0.01	4	2.64	10	0.00	0
7855.131209	P 9 P 9	3.7758E-26	16	0.05118	2	-1.93	1	4.04	2	0.37	3	1.77	12	0.00	0
7857.076680	P 9 Q 8	5.2353E-26	24	0.05111	2	-1.91	1	3.92	2	0.25	3	1.37	8	0.00	0
7858.323972	O 5 P 4	7.3792E-27	26	0.05875	2	-1.46	1	4.24	6	0.39	5	1.97	26	0.00	0
7861.470477	P 7 P 7	3.2974E-26	5	0.05311	2	-1.75	1	3.96	2	0.29	2	2.20	8	0.00	0
7863.443990	P 7 Q 6	4.9933E-26	14	0.05295	2	-1.84	1	3.58	2	-0.00	3	2.88	12	0.00	0
7867.195268*	Q29 P30	3.5806E-28	30	0.03214	14	-2.29	14	5.85	30	0.76	27	4.81	175	0.00	0
7867.276527*	Q27 Q27	3.2429E-27	36	0.03390	2	-2.66	2	4.01	4	0.22	4	4.36	21	0.00	0
7867.653770	P 5 P 5	2.2153E-26	4	0.05616	2	-1.51	1	4.20	2	0.38	2	1.83	8	0.00	0
7869.418793	Q25 Q25	6.2910E-27	49	0.03577	4	-2.45	3	4.11	9	0.37	10	3.50	47	-3.63	59
7869.665367	P 5 Q 4	3.9708E-26	9	0.05613	2	-1.93	1	3.91	2	-0.01	6	3.08	9	0.00	0
7871.206534*	Q25 R24	1.7995E-27	12	0.03417	14	-2.50	3	4.18	8	0.36	9	4.78	43	0.00	0
7871.394045	Q23 Q23	1.1412E-26	4	0.03759	2	-2.42	1	4.05	2	0.11	2	3.08	13	-5.13	13
7871.612422	Q25 P26	1.4192E-27	12	0.03553	16	-2.64	6	4.02	17	0.08	17	4.40	95	-10.93	107
7873.203566	Q21 Q21	1.9654E-26	7	0.03992	2	-2.50	1	4.40	2	0.71	2	3.20	10	-3.78	11

7873.569675	Q23 P24	2.5586E-27	20	0.03655	10	-2.35	5	4.22	13	0.39	14	3.49	70	-2.95	80
7873.680414	P 3 P 3	6.9906E-27	32	0.06143	8	-0.61	7	4.65	8	0.55	64	2.22	41	0.00	0
7874.848492	Q19 Q19	3.1271E-26	9	0.04168	2	-2.21	1	3.66	2	0.07	2	3.18	8	-5.27	8
7875.027182	Q21 R20	5.6873E-27	19	0.03932	6	-2.33	3	2.95	9	0.40	9	5.69	39	-8.28	43
7875.361015	Q21 P22	4.3188E-27	17	0.03898	6	-2.51	4	3.41	11	0.14	12	5.03	51	-12.55	58
7875.764694	P 3 Q 2	1.9123E-26	8	0.06055	2	-0.61	3	4.40	4	0.23	13	2.74	15	0.00	0
7876.329883	Q17 Q17	4.6897E-26	15	0.04352	2	-2.07	1	3.65	2	0.03	2	2.71	7	-5.22	7
7876.690465	Q19 R18	9.2347E-27	26	0.04101	4	-2.31	2	3.30	7	0.20	8	5.24	32	-10.64	33
7876.987555	Q19 P20	6.8532E-27	23	0.04101	4	-2.38	3	3.65	9	0.08	10	4.73	43	-11.07	45
7877.648684	Q15 Q15	6.5657E-26	23	0.04542	2	-1.93	1	3.96	2	0.20	2	1.86	9	-5.77	8
7878.190625	Q17 R16	1.4109E-26	6	0.04350	2	-2.02	3	4.18	9	0.44	9	2.91	44	-4.55	43
7878.450299	Q17 P18	1.0157E-26	3	0.04320	4	-2.00	4	3.82	13	0.50	13	3.87	60	-4.93	58
7878.805739	Q13 Q13	8.5471E-26	27	0.04709	4	-1.88	1	4.21	2	0.03	2	1.38	9	-6.85	7
7879.528760	Q15 R14	2.0115E-26	6	0.04511	2	-1.97	6	3.58	20	0.30	21	3.82	91	-7.30	86
7879.750063	Q15 P16	1.3950E-26	6	0.04485	2	-2.30	9	3.85	28	0.09	30	3.53	132	0.00	0
7879.801772	Q11 Q11	1.0272E-25	5	0.04878	2	-1.65	1	4.59	5	0.23	5	1.33	27	-1.15	17
7880.637426	Q 9 Q 9	1.1345E-25	8	0.05018	2	-1.54	2	4.35	8	0.46	9	0.97	41	-11.11	29
7880.705990*	Q13 R12	2.6465E-26	52	0.04712	2	-2.11	4	2.61	7	0.12	14	4.94	42	0.00	0
7880.887550	Q13 P14	1.7695E-26	6	0.04665	2	-2.01	13	2.78	47	0.16	50	4.73	197	-8.54	185
7881.313229	Q 7 Q 7	1.1141E-25	4	0.05138	2	-1.54	2	4.00	7	0.10	7	2.15	33	-4.33	25
7881.723516	Q11 R10	3.3388E-26	12	0.04834	2	-1.85	3	2.73	10	0.21	10	4.59	40	-16.15	46
7881.829596	Q 5 Q 5	9.4681E-26	167	0.05395	2	-1.48	1	3.83	4	0.10	4	3.10	18	-7.74	17
7881.863196*	Q11 P12	2.0528E-26	117	0.04809	4	-0.98	4	4.51	12	0.52	13	1.54	62	0.00	0

7882.186894	Q 3 Q 3	6.0835E-26	71	0.05779	2	-1.00	2	4.09	8	-0.07	11	3.47	28	37.89	11
7882.582895	Q 9 R 8	3.9006E-26	16	0.05029	2	-1.55	2	5.65	7	0.34	10	0.49	32	-0.41	15
7882.677176	Q 9 P10	2.1652E-26	14	0.05022	2	-1.55	3	1.26	12	0.15	14	6.07	37	1.97	27
7883.286730	Q 7 R 6	4.1654E-26	23	0.05194	2	-1.57	2	3.62	10	0.22	14	3.89	36	-15.92	14
7883.329114	Q 7 P 8	1.9902E-26	24	0.05182	2	-0.87	3	4.97	12	0.65	11	0.99	42	32.29	30
7883.817345*	Q 5 P 6	1.4924E-26	35	0.05450	4	-3.06	4	5.85	13	0.07	12	2.75	42	0.00	0
7883.841192	Q 5 R 4	4.1331E-26	25	0.05310	2	-0.91	2	4.78	9	0.28	11	3.23	33	90.01	14
7884.136458	Q 3 P 4	7.6346E-27	63	0.05819	8	-0.59	6	5.54	21	0.46	22	1.61	105	42.27	75
7884.271210	Q 3 R 2	3.8093E-26	29	0.05820	2	-0.86	2	3.14	8	0.28	9	4.20	30	27.45	15
7888.056508	R 1 R 1	6.7507E-26	26	0.05686	2	-0.99	1	4.13	4	-0.11	6	2.93	18	0.00	0
7889.933310	R 1 Q 2	1.7549E-26	7	0.06072	2	-0.34	1	4.60	4	-0.89	4	2.57	18	0.00	0
7893.528305	R 3 R 3	7.8504E-26	50	0.05602	2	-0.74	1	3.14	4	0.10	6	4.68	14	0.00	0
7895.477879	R 3 Q 4	4.1264E-26	20	0.05636	2	-0.49	1	3.83	6	0.16	5	3.57	22	0.00	0
7898.439793	S 1 R 2	3.5296E-26	9	0.05915	4	0.36	4	5.13	14	0.52	14	1.29	74	0.00	0
7898.839273	R 5 R 5	8.6343E-26	25	0.05283	2	-1.04	1	3.61	6	-0.35	6	3.63	34	0.00	0
7900.827017	R 5 Q 6	5.6255E-26	27	0.05287	2	-0.84	1	3.49	2	-0.09	3	3.51	12	0.00	0
7903.988208	R 7 R 7	8.6785E-26	51	0.05073	2	-0.97	1	3.52	6	0.01	6	2.95	32	0.00	0
7906.004093	R 7 Q 8	6.3057E-26	28	0.05077	2	-0.90	1	3.43	2	0.02	3	2.79	16	0.00	0
7908.973798	R 9 R 9	8.0428E-26	31	0.04927	2	-1.08	1	3.37	2	-0.08	3	3.16	14	0.00	0
7909.653719	S 3 R 4	4.2863E-26	18	0.05522	2	-0.09	1	3.74	4	-0.27	5	2.93	22	0.00	0
7911.013561	R 9 Q10	6.2274E-26	32	0.04921	2	-1.15	1	2.97	4	-0.10	4	3.76	16	0.00	0
7913.794639	R11 R11	6.8996E-26	49	0.04778	2	-1.32	1	3.01	4	0.02	4	4.40	16	0.00	0
7915.856072	R11 Q12	5.5820E-26	23	0.04784	2	-1.28	1	3.42	2	0.08	3	2.92	12	0.00	0

Acknowledgements
The authors acknowledge the financial support from CNES.

References

[1] Bertaux JL, Hauchecorne A, Lefèvre F, Jouglet D, Blanot L, Bréon FM, Akaev P, Lafrique P. Use of the 1.27 µm O_2 absorption band for CO_2 and methane estimates in nadir viewing from space: Potential and application to Microcarb. Geophys. Res. Abstracts **20**, EGU2018-14935, EGU General Assembly (2018).

[2] Sun K, Gordon IE, Sioris CE, Liu X, Chance K, Wofsy SC. Re-evaluating the use of O_2 $a^1\Delta_g$ band in the spaceborne remote sensing of greenhouse gases. The combined 15th HITRAN and 14th ASA conference (Cambridge, MA) (2018)

[3] Washenfelder RA, Toon GC, Blavier JF, Yang Z, Allen NT, Wennberg PO, Vay SA, Matross DM, Daube BC. Carbon dioxide column abundances at the Wisconsin Tall Tower site. J Geophys Res 2006; 111, D22305, doi:10.1029/2006JD007154.

[4] Gordon IE, Kassi S, Campargue A, Toon GC. First identification of the $a^1\Delta_g - X^3\Sigma_g^-$ electric quadrupole transitions of oxygen in the solar and laboratory spectra. J Quant Spectrosc Radiat Transf 2010;111:1174-83.

[5] Mendonca J, Strong K, Wunch D, Toon GC, Long DA, Hodges JT, Sironneau VT, Franklin JE. Using a speed-dependent Voigt line shape to retrieve O_2 from Total Carbon Column Observing Network solar spectra to improve measurements of XCO_2. Atmos Meas Tech 2019;12:35–50. https://doi.org/10.5194/amt-12-35-2019

[6] Long DA, Havey DK, Okumura M, Miller CE, Hodges JT. O_2 A-band line parameters to support atmospheric remote sensing. J Quant Spectrosc Radiat Transf 2010;111:2021-36. doi.org/10.1016/j.jqsrt.2010.05.011

[7] Wunch D, Toon GC, Blavier JF, Washenfelder RA, Notholt J, Connor BJ, et al. The Total Carbon Column Observing Network. Philos Trans Royal Soc A 2011;369:2087–2112. doi.org/10.1098/rsta.2010.0240

[8] Goody RM, Yung YL. Atmospheric Radiation. Theoretical Basis. Second edition. Oxford University Press, New York, **xvi, 519** (1989) Science **247**, 4941, 476-476 (1990). doi.org/10.1126/science.247.4941.476

[9] microcarb.cnes.fr/en

[10] Mondelain D, Kassi S, Campargue A. Accurate laboratory measurement of the O_2 collision-induced absorption band near 1.27 µm. J Geophys Res 2019;124 :414-23. doi.org/10.1029/2018JD029317

[11] Konefal M, Kassi S, Mondelain D, Campargue A. High sensitivity spectroscopy of the O_2 band at 1.27 µm: (I) Spectroscopic parameters of the lines above 7920 cm^{-1}. Sumitted to J Quant Spectrosc Radiat Transf, 2019.

[12] Leshchishina O, Kassi S, Gordon IE, Rothman LS, Wang L, Campargue A. High sensitivity CRDS of the $a^1\Delta_g - X^3\Sigma_g^-$ band of oxygen near 1.27 µm: extended observations, quadrupole transitions, hot bands and minor isotopologues. J Quant Spectrosc Radiat Transf 2010;111:2236-45.

[13] Leshchishina O, Kassi S, Gordon IE, Yu S, Campargue A. The $a^1\Delta g - X^3\Sigma$-g band of $^{16}O^{17}O$, $^{17}O^{18}O$ and $^{17}O_2$ by high sensitivity CRDS near 1.27 μm. J Quant Spectrosc Radiat Transf 2011;112:1257-65. doi.org/10.1016/j.jqsrt.2010.05.014

[14] Tran DD, Sironneau VT, Hodges JT, Armante R, Cuesta J, Tran H. Prediction of high-order line-shape parameters for air-broadened O 2 lines using requantized classical molecular dynamics simulations and comparison with measurements. J Quant Spectrosc Radiat Transf 2019;222–223:108–114.

[15] Brown LR, Plymate C. Experimental Line Parameters of the Oxygen A Band at 760 nm. J Mol Spectrosc 2000;199:166 –179.

[16] Hartmann JM, Sironneau V, Boulet C, Svensson T, Hodges JT, Xu CT: Collisional broadening and spectral shapes of absorption lines of free and nanopore-confined O_2 gas. Phys Rev A 2013;87:032510. https://doi.org/10.1103/PhysRevA.87.032510, 2013.

[17] Lamouroux J, Sironneau V, Hodges JT, Hartmann JM: Isolated line shapes of molecular oxygen: Requantized classical molecular dynamics calculations versus measurements. Phys Rev A 2014;89:042504. https://doi.org/10.1103/PhysRevA.89.042504.

[18] Drouin BJ, Benner DC, Brown LR, Cich MJ, Crawford TJ, Devi VM, Guillaume A, Hodges JT, Mlawer EJ, Robichaud DJ, Oyafuso F, Payne VH, Sung K, Wishnow EH, Yu S. Multispectrum analysis of the oxygen A-band. J Quant Spectrosc Radiat Transf 2017;186:118-138. https://doi.org/10.1016/j.jqsrt.2016.03.037

[19] Domysławska J, Wójtewicz SZ, Masłowski P, Cygan A, Bielska K, Trawiński RS, Ciuryło R, Lisak D. Spectral line shapes and frequencies of the molecular oxygen B-band R-branch transitions. J Quant Spectrosc Radiat Transf 2015;155 :22-31. doi.org/10.1016/j.jqsrt.2014.12.015.

[20] Mondelain D, Kassi S, Sala T, Romanini D, Marangoni M, Campargue A. Sub-MHz accuracy measurement of the S(2) 2–0 transition frequency of D_2 by comb-assisted cavity ring down spectroscopy J Mol Spectrosc 2016;326:5-8. doi:10.1016/j.jms.2016.02.008

[21] Mondelain D, Mikhailenko SN, Karlovets EV, Béguier S, Kassi S, Campargue A. Comb-Assisted Cavity Ring Down Spectroscopy of ^{17}O enriched waterbetween 7443 and 7921 cm^{-1}. J Quant Spectrosc Radiat Transf 2017;203:206-12. 10.1016/j.jqsrt.2017.03.029

[22] Gordon IE, Rothman LS, Hill C, Kochanov RV, Tan Y, Bernath PF, Birk M, Boudon, CampargueA, Chance KV, Drouin BJ, Flaud JM, Gamache RR, Hodges JT, Jacquemart D, Perevalov VI, Perrin A, Shine KP, Smith MAH, Tennyson J, Toon GC, Tran H, Tyuterev VG, Barbe A, Császár AG, Devi VM, Furtenbacher T, Harrison JJ, Hartmann J-M, Jolly A, Johnson TJ, Karman T, Kleiner I, Kyuberis AA, Loos J, Lyulin OM, Massie ST, Mikhailenko SN, Moazzen-Ahmadi N, Müller HSP, Naumenko OV, Nikitin AV, Polyansky OL, Rey M, Rotger M, Sharpe SW, Sung K, Starikova E, Tashkun SA, Vander Auwera J, Wagner G, Wilzewski J, Wcisło P, Yu S, Zak EJ. The HITRAN2016 molecular spectroscopic database. J Quant Spectrosc Radiat Transf 2017;203:3–69. doi:10.1016/j.jqsrt.2017.06.038.

[23] Delahaye T, Maxwell SE, Reed ZD, Lin H, Hodges JT, Sung K, Devi VM, Warneke T, Spietz P, Tran H. Precise methane absorption measurements in the 1.64 μm spectral region for the MERLIN mission. J Geophys Res 2016;121:7360-70, doi: 10.1002/2016JD025024.

[24] Ngo NH, Lin H, Hodges JT, Tran H. Spectral shapes of rovibrational lines of CO broadened by He, Ar, Kr and SF6: A test case of the Hartmann-Tran profile. J Quant Spectrosc Radiat Transf 2017;203:325-33.

[25] Nelkin M, Ghatak A. Simple binary collision model for Van Hove's Gs(r,t)+. Phys Rev 1964;135:A4-A9.

[26] Rohart F, Mader H, Nicolaisen HW. Speed dependence of rotational relaxation induced by foreign gas collisions: studies on CH_3F by millimeter wave coherent transients. J Chem Phys 1994; 101: 6475-86.

[27] Rohart F, Ellendt A, Kaghat F, Mäder H. Self and polar foreign gas line broadening and frequency shifting of CH_3F: effect of the speed dependence observed by millimeter-wave coherent transients. J Mol Spectrosc 1997;185:222-33.

[28] Ngo NH, Lisak D, Tran H, Hartmann JM. An isolated line shape model to go beyond the Voigt profile in spectroscopic databases and radiative transfer codes. J Quant Spectrosc Radiat Transf 2013;129:89-100.

[29] Tennyson J, Bernath PF, Campargue A, Csaszar AG, Daumont L, Gamache RR, Hodges JT, Lisak D, Naumenko OV, Rothman LS, Tran H, Zobov NF, Buldyreva J, Boone DC, Hartmann JM, McPheat R, Weidmann D, Murray J, Ngo NH, Polyansky OL. Recommended isolated-line profile for representing high-resolution spectroscopic transitions. Pure Appl Chem 2014;86:1931-43.

[30] Rosenkranz PK. Shape of the 5 mm oxygen band in the atmosphere. IEEE Trans Antennas Propag 1975;23:498-506.

[31] Rautian SG and Sobel'man II. The effect of collisions on the Doppler broadening of spectral lines, Sov Phys Usp 1967;9:701-16.

[32] Newman SM, Orr-Ewing AJ, Newnham DA, Ballard J. Temperature and pressure dependence of line widths and integrated absorption intensities for the O_2 $a^1\Delta_g$ - $X^3\Sigma_g$ - (0,0) transition. J Phys Chem 2000;A1049467.

[33] Yang Z, Wennberg PO, Cageao RP, Pongetti TJ, Toon GC, Sander S P. Ground-based photon path measurements from solar absorption spectra of the O_2 A-band. J Quant Spectrosc Radiat Transf 2005;90:309-21.

[34] Lisak D, Cygan A, Bermejo D, Domenech JL, Hodges JT, Tran H. Application of the Hartmann-Tran profile to analysis of H_2O spectra. J Quant Spectrosc Radiat Transf 2015;164:221–230.

[35] Le T, Fissiaux L, Lepère M, Tran H. Isolated line shape of methane with various collision partners. J Quant Spectrosc Radiat Transf 2016;185:27–36.

[36] Wójtewicz S, Masłowski P, Cygan A, Wcisło P, Zaborowski M, Piwiński M, Ciuryło R, Lisak D. Speed-dependent effects and Dicke narrowing in nitrogen-broadened oxygen. J Quant Spectrosc Radiat Transf 2015;165:68–75.

[37] Robichaud DJ, Hodges JT, Brown LR, Lisak D, Masłowski P, Yeung LY, Okumura M, Miller CE. Experimental intensity and lineshape parameters of the oxygen A-band using frequency-stabilized cavity ring-down spectroscopy. J Mol Spectrosc 2008;248:1–13.

[38] Long DA, Hodges JT. On spectroscopic models of the O_2 A-band and their impact upon atmospheric retrievals. J Geophys Res 2012; 117:D12309. doi:10.1029/2012JD017807.

[39] Herzberg L, Herzberg G. Fine structure of the infrared atmospheric oxygen bands. Astrophys. J 1947;105:353-9.